Measurement of Helicon Waves With Phase Contrast Imaging on DIII-D – A Theoretical Feasibility Study

S. S. Denk,[1, 2, a)] C. Lau,[3] J. C. Rost,[1] A. Marinoni,[1] R. I. Pinsker,[2] and M. Porkolab[1]

[1)] *Plasma Science and Fusion Center, Massachusetts Institute of Technology, Cambridge, MA, United States of America*
[2)] *General Atomics, San Diego, CA, United States of America*
[3)] *Oak Ridge National Laboratory, Oak Ridge, TN, United States of America*

[a)] *Corresponding author:denks@fusion.gat.com*

Abstract. A DIII-D high-beta H-mode discharge, with $I_p = 850\,\mathrm{kA}$, $B_t = 2.1\,\mathrm{T}$ $n_e = 4 \times 10^{19}\,\mathrm{m}^{-3}$, has been designed to validate full wave modeling of helicon waves by optimizing the expected response of the Phase Contrast Imaging diagnostic. Helicon waves have been predicted to have high current drive efficiency off-axis without facing the accessibility issues of lower-hybrid waves. To test these predictions experimentally, DIII-D has recently commissioned a high-power helicon antenna. To confidently predict the behavior of helicon waves in future devices, measurements of their fundamental properties and validation against models will be essential. Phase contrast imaging (PCI) is an absolutely calibrated internal reference interferometer able to measure density fluctuations with radial wavenumbers k_R between $1.5\,\mathrm{cm}^{-1}$ and $20\,\mathrm{cm}^{-1}$. For helicon waves $2\,\mathrm{cm}^{-1} < k_R < 10\,\mathrm{cm}^{-1}$ is expected, allowing PCI to measure their envelope and wavenumber spectrum. This makes PCI a powerful tool for the validation of state-of-the-art models, like the AORSA full wave code. AORSA is used to compute the density perturbations measured by the PCI with 2D calculations corresponding to 11 different toroidal mode numbers combined to resolve the trajectory of the helicon wave in 3D. This is necessary because the waves travel 120 degrees toroidally from the antenna to the PCI. A cold plasma finite element model (CPFEM) [4] is used to predict propagation through the scrape-off layer. The result of the CPFEM model is connected to AORSA by creating an artificial Gaussian antenna on the last closed flux surface. PCI shows best results for waves with small vertical wavenumbers k_z. Modeling the helicon waves for several past DIII-D experiments shows that k_z is minimized if the intersection of the helicon and the PCI laser beams occurs in the midplane. For such an optimized scenario the predicted signal level is two orders of magnitude larger than the background density fluctuations arising from broadband turbulence.

INTRODUCTION

It has been shown that steady-state operation in tokamaks requires external current drive sources, which supplement and enhance the bootstrap current [1, 2]. Hence, actuators for the efficient current drive are crucial for the design of a steady-state fusion power plant based on the tokamak scheme. Simulations have identified the potential of the helicon wave as an efficient current drive actuator in high-beta plasmas on DIII-D [3] and ITER [4]. To confirm these predictions at reactor-relevant power levels a traveling wave antenna has been recently installed and commissioned at DIII-D [5]. The primary goal of this undertaking is the confirmation of the predicted current drive efficiency via current measuring diagnostics such as the motional stark effect diagnostic [6]. Confident extrapolation from the observations at the DIII-D tokamak to future machines requires validated predictions including the coupled RF power, the wave propagation, and the wavenumber spectrum in the core. Phase contrast imaging (PCI) can provide an absolutely calibrated measurement of the line-integrated RF electron density fluctuation in the core plasma which can be compared to results of 3 dimensional full-wave RF codes, allowing the assessment of the propagation path, the absolute amplitude, the radial envelope, and the perpendicular wavenumber of the helicon wave. This complements the suite of diagnostics that will study various helicon parameters at different locations in the plasma [7]. While PCI measurement of RF waves has been successfully demonstrated in the past [8, 9, 10], application to measurement of the helicon introduces technical and operational challenges, including development of a novel modulation scheme applicable to higher frequencies [11] and design of a dedicated validation study which steers the extremely localized helicon beam to intersect the PCI laser while optimizing the expected diagnostic response. The plasma optimized for validation studies (described below) lies within established DIII-D parameter ranges and helicon design parameters, but is not a high current drive scenario.

In this paper full-wave calculations of the helicon waves are used to demonstrate that PCI can detect helicon waves in a realistic DIII-D experiment under the assumption of a quiescent scrape-off layer (SOL). One potential concern is the impact of the background turbulence on the measurement. However, the synthetic helicon wave signals are over two orders of magnitude larger than the turbulent signals observed in the reference discharge used for the modeling. In the next section the PCI diagnostic is briefly introduced. Afterward, a DIII-D experiment optimized

for PCI measurements of helicon waves is presented, and the expected PCI response in this experiment is discussed. Conclusions are drawn at the end of the paper.

The PCI diagnostic

PCI is an imaging interferometer that measures plasma density fluctuations integrated along a vertical laser beam with sub-mm resolution across the beam. A detailed description of the DIII-D PCI system can be found in Ref. [11] and references therein. The geometry of the laser beam along which the density fluctuations are integrated is depicted in Fig. 1 below. The line integration restricts the PCI response to waves roughly perpendicular to the vertical laser beam, i.e. the vertical component of the wavelength λ_z should not be much smaller than the size of the interaction region between the fluctuation and the laser.

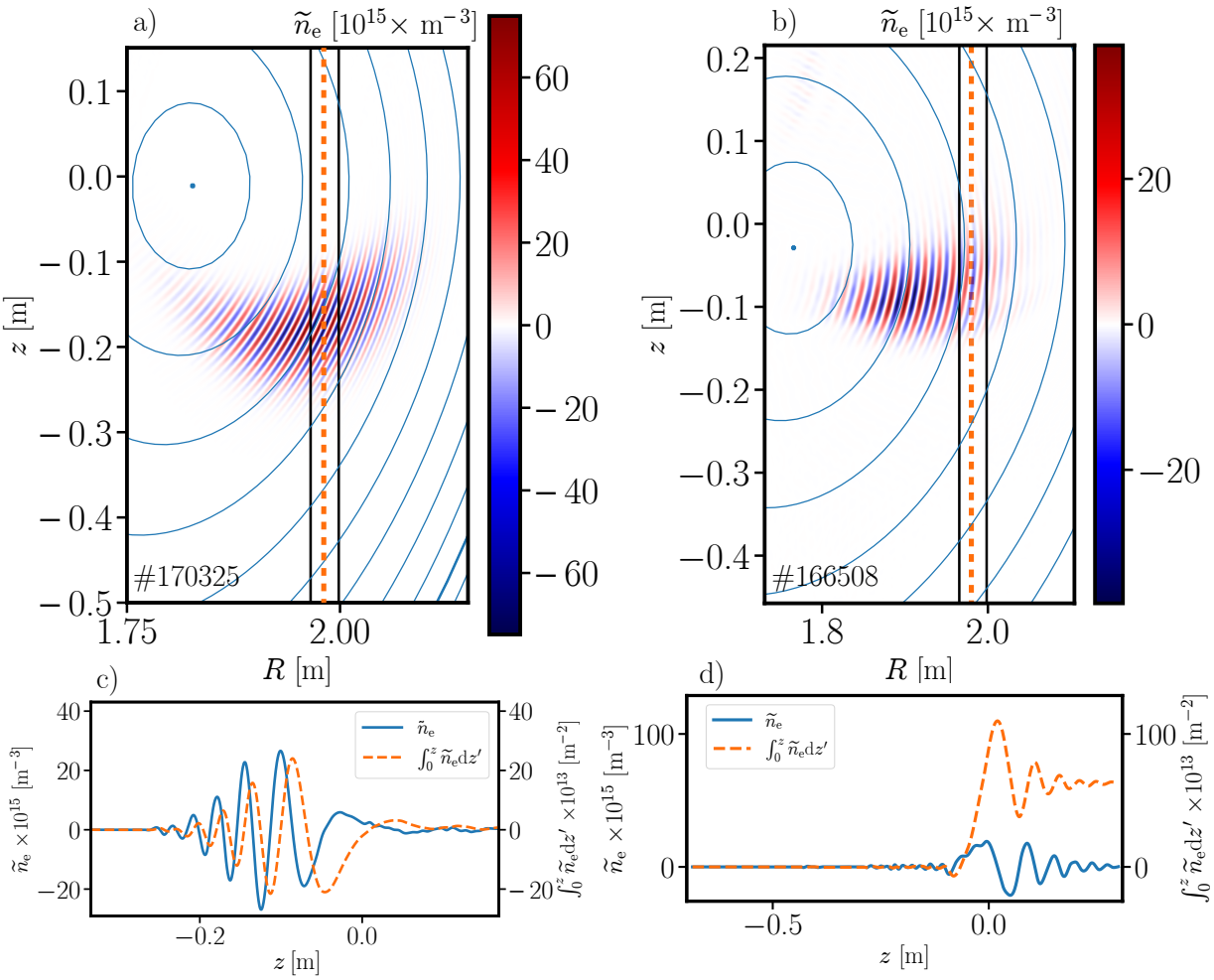

FIGURE 1. Density perturbations due to the helicon wave computed by AORSA evaluated at the toroidal location of the DIII-D PCI diagnostic. The vertical dashed orange line shows the center of the PCI laser eam, with black lines showing the radial width. (a) Density perturbation for a helicon injected into a discharge similar to DIII-D shot #170325, where the B_t was reversed and I_p reduced from 1 MA to 800 kA to facilitate an intersection between PCI and helicon. (b) Perturbation is expected in an optimized discharge developed from shot #166508. (c) Evaluation of the fluctuating density along the central PCI chord shown in (a), integrating to a negligible signal level. (d) Evaluation of the density along the central PCI chord of the optimized discharge shows that the integrated value is dominated by the central tangent wave.

The DIII-D PCI employs a photoconductive detector, which restricts the frequency bandwidth to 2 MHz. In order to

detect the helicon wave at 476 MHz a laser modulation system based on a novel electro-optic modulator [12] is being integrated into the system, which will operate at 475 MHz and allow heterodyne detection of the density perturbations of the helicon beam.

To predict the response of the PCI diagnostic it is necessary to resolve the $\tilde{n}_e$ associated with the helicon wave in 3D, hence full-wave computations are required. Note that the cold plasma approximation is insufficient to accurately estimate $\tilde{n}_e$ for helicon waves in the DIII-D core. In addition, a solution correct to all orders in the finite ion-Larmor-radius parameter $k_\perp \rho_i$ is required because $k_\perp \rho_i \sim 1$ for the helicon. The all-orders spectral algorithms (AORSA) code [13] was therefore chosen as best fulfilling all these requirements.

The computation costs of using AORSA however are significant. A single 2D calculation with the resolution necessary for helicon waves can easily consume 100k CPU hours. Resolution in 3D is achieved by decomposing the wave into individual toroidal modes. Calculation of 11 modes has been found to accurately represent the 3D path, envelope, and wave structure of the helicon in the core plasma.

It is not feasible for a single model to calculate the wave continuously from the antenna, through the SOL, and across the core plasma due to the difference in wavenumbers and parameter scale lengths, as well as the complexity of the antenna structure [4]. The computation domain is therefore split into two regions. In the unconfined region a cold plasma finite element model (CPFEM) [14] is used to predict the wave propagation between the antenna and the last closed flux surface. Similarly to AORSA, this is a 2D model, and toroidal mode number decomposition is used to achieve 3D resolution. The two calculations are interfaced with each other by using the current at the last closed flux surface (LCFS) calculated by the CPFEM as a boundary condition to AORSA, which can be thought of as a virtual antenna. The CPFEM assumes a toroidally symmetric antenna that is perfectly aligned with the helicity of magnetic field to limit the excitation of the slow wave. To accurately solve the coupling problem a 3D full-wave model with a realistic antenna is needed, but at the time of writing such a model is not readily available. Preliminary calculations with a reduced model [15] indicate that slow-wave excitation may not be insignificant for the optimized experiment discussed below. While we normalize the electric fields such that a total power of 800 kW is absorbed here, the helicon wave could still be detected even if only half of this power is coupled to the fast wave. To assure that the helicon beam is approximately Gaussian-shaped at the interface layer a static, poloidally symmetric density profile is assumed in the SOL. It is expected that turbulent density fluctuations in the SOL will have some effect on the synthetic PCI measurements [17]. Hence, a quantitative study of this as well as the effect of realistic antenna-plasma coupling will be subject of future investigations.

The toroidal and poloidal envelope of the current computed by the CPFEM at the LCFS is shown in Fig. 2(a). A virtual antenna parameterized as a 2D Gaussian provides a good representation of the dominant peak, while the side lobes can be neglected. The residual error of the total calculated current minus the virtual antenna current is shown in Fig. 2(b).

PREDICTED PCI MEASUREMENTS OF HELICON WAVES IN AN OPTIMIZED DIII-D EXPERIMENT

Maximization of the PCI signal from the helicon wave requires that the waves propagate perpendicular to the PCI beam in the interaction region. As shown in Fig. 1, the wavefronts of the helicon are nearly parallel to the flux surfaces, resulting in a requirement that the helicon wave intersects the PCI beam near the midplane. Parameter scans with the GENRAY code [16] identified the toroidal magnetic field B_t, the plasma current I_p, the electron density n_e and the plasma shape as possible actuators for steering the beam. By mining the DIII-D database of previous discharges, shot #166508 was identified as an ideal scenario with only minor adjustments required. This discharge exhibited high β_p with 8 MW of neutral beam heating at a high magnetic field of 2.18 T and a moderate current of 850 kA. Optimization for PCI helicon measurements entailed reversing the magnetic field so the helicon waves propagate towards the PCI toroidally, increasing the elongation, and reducing n_e by 15 % to $4.8 \times 10^{19}\,\mathrm{m}^{-3}$. In this configuration, the helicon waves drive counter current. The necessity of optimizing the discharge for PCI detection of the helicon wave is demonstrated in Fig. 1, which shows the calculated $\tilde{n}_e$ at the PCI toroidal location. A plasma with non-optimized parameters is shown in Fig. 1(a), where the helicon intersects the PCI beam 20 cm below the midplane. The wavefronts are not perpendicular to the vertical PCI laser, and the line-integrated signal is negligible. A fully optimized discharge is represented in Fig. 1(b), with the helicon/PCI intersection at the midplane and wavefronts tangent to the PCI beam, producing a large PCI signal. The inclusion of additional physical processes, such as wave distortions due to plasma edge turbulence [17] or parametric decay instabilities [18], are expected to quantitatively affect the expected PCI signal from helicon waves both on and off the midplane. It is anticipated that fine-tuning of

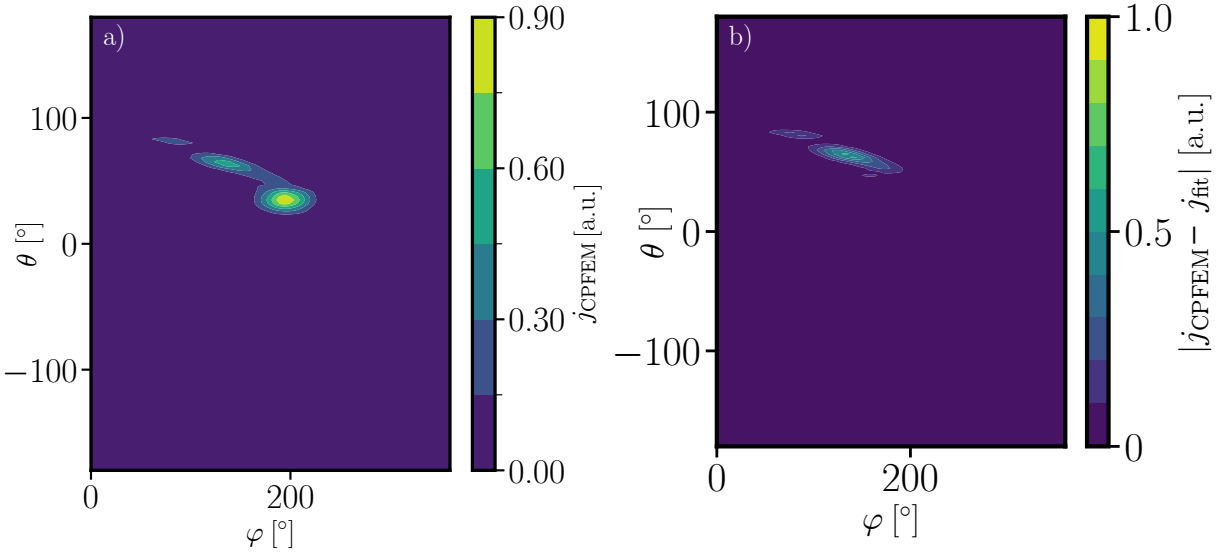

FIGURE 2. (a) Helicon wave currents on the LCFS as computed by the CPFEM. (b) Residual difference between the full calculation of the currents at the LCFS and the virtual antenna representation, showing that the central peak is well captured but the side lobes are neglected.

the discharge will be required in practice, and design is underway for a set of parameter sweeps designed to allow optimal measurements given parameter uncertainties.

Estimating the signal-to-noise ratio of the helicon signals requires a measure of the expected background. The heterodyne detection process will produce a signal that combines the helicon signal mixed from 476 MHz down to 1 MHz and homodyne detection of the low-frequency broadband turbulence. A laser modulation of 100% is assumed, and the expected signal due to the helicon as calculated above is combined with the PCI broadband turbulence measurement acquired during the experimental discharge from which the optimized scenario was developed. In order to produce a conservative estimate, the center 3 PCI channels were averaged over a 10 ms window, producing the turbulence $S(f)$ spectrum shown in Fig. 3(a). This is combined with the expected helicon signal to produce Fig. 3(b), which shows the helicon signal several orders of magnitude above the signal from turbulent fluctuations. Hence, the signal corresponding to the helicon wave can be easily detected by the PCI even if much less than the here assumed 800 kW are coupled to the fast wave or if the modulation of the laser is less efficient. Improved discrimination of the helicon signal can be achieved with longer averaging and spectral reconstruction. Figure 3(c) shows the expected $S(k, f)$ based on 100 ms of data in 128 µs windows from 12 spatial channels, with the quantitative comparison at 1 MHz shown in Fig. 3(d). The measured wavenumber $-4\,\mathrm{cm}^{-1}$ agrees well with the maximum k_R that can be directly derived from the AORSA calculations.

CONCLUSIONS

To predict the propagation of the helicon waves from the antenna to the core, the helicon wave propagation in a poloidally symmetric scrape-off layer is computed with a cold plasma finite element model. The results of this model are coupled to the AORSA code via a Gaussian-shaped virtual antenna located on the last closed flux surface. The AORSA code directly delivers the $\tilde{n}_\mathrm{e}$ predictions needed to compute synthetic PCI signals.

Achieving the largest helicon signal on the PCI requires that the helicon wavefronts be tangent to the PCI laser beam, which is achieved by placing the PCI/helicon intersection at the midplane. An optimized discharge has been developed based on minor modifications of DIII-D shot #166508.

For this optimized experiment the synthetic PCI measurements of the helicon waves have been compared against the turbulent background measured in the reference discharge #166508. The synthetic helicon wave signal exceeds the turbulent background by more than two orders of magnitude. Furthermore, the wavenumber spectrum computed from the mixture of synthetic and measured signals agrees with the spectrum derived directly from the AORSA

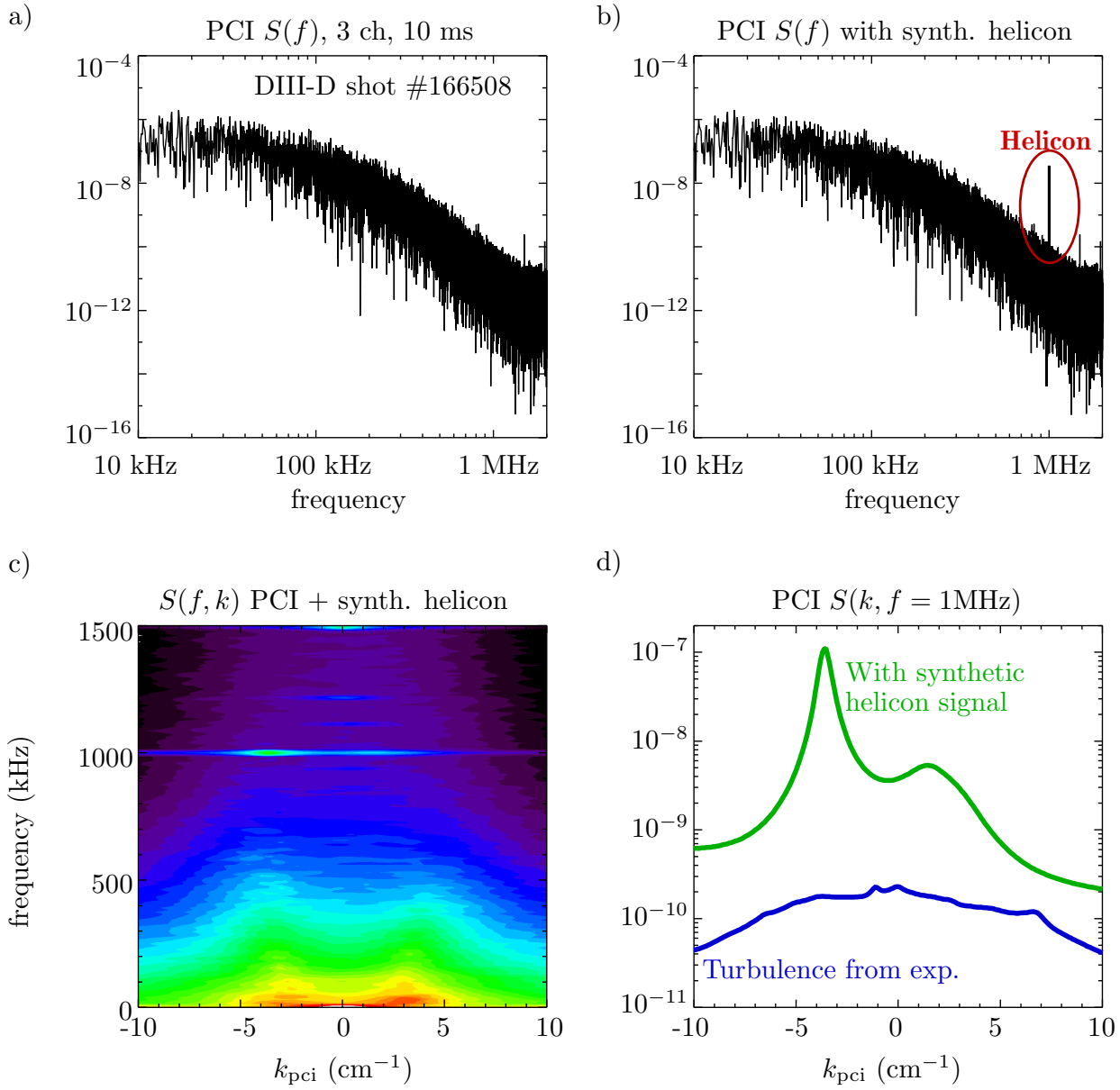

FIGURE 3. (a) Experimentally measured PCI turbulence spectrum from discharge #166508, the basis of the idealized scenario, using 1 ms of data from 3 PCI channels. (b) Experimental $S(f,t)$ with the expected level of the heterodyned helicon perturbation, as calculated from AORSA and a synthetic PCI calculation. (c) $S(k,f)$ spectrum of PCI data with expected synthetic helicon signal added, based on 100 ms of data across 12 spatial channels. (d) $S(k, f = 1\,\mathrm{MHz})$ comparing experimental data in blue to the combined experiment and synthetic signal in green, showing the helicon signal 3 orders of magnitude larger than the homodyne turbulence signal.

calculation. Heterodyned PCI is predicted to be capable of detecting the Helicon density fluctuations with particular plasma parameters and has the potential to validate the cold plasma-AORSA model.

ACKNOWLEDGMENTS

This material is based upon work supported by the U.S. Department of Energy, Office of Science under Award(s) DE-FC02-04ER54698, DE-SC0016154 and DE-AC05-00OR22725.

REFERENCES

1. F. Najmabadi, A. Abdou, L. Bromberg, T. Brown, V. Chan, M. Chu, F. Dahlgren, L. El-Guebaly, P. Heitzenroeder, D. Henderson, H. E. St. John, C. E. Kessel, L. L. Lao, G. R. Longhurst, S. Malang, T. K. Mau, B. J. Merrill, R. L. Miller, E. Mogahed, R. L. Moore, T. Petrie, D. A. Petti, P. Politzer, A. R. Raffray, D. Steiner, I. Sviatoslavsky, P. Synder, G. M. Syaebler, A. D. Turnbull, M. S. Tillack, L. M. Waganer, X. Wang, P. West, and P. Wilson, "The ARIES-AT advanced tokamak, advanced technology fusion power plant," Fusion Eng. Des. **80**, 3 (2006), https://www.sciencedirect.com/science/article/pii/S0920379605007210.
2. B. N. Sorbom, J. Ball, T. R. Palmer, F. J. Mangiarotti, J. M. Sierchio, P. Bonoli, C. Kasten, D. A. Sutherland, H. Barnard, C. B. Haakonsen, *et al.*, "ARC: A compact, high-field, fusion nuclear science facility and demonstration power plant with demountable magnets," Fusion Eng. Des. **100**, 378 (2015), https://www.sciencedirect.com/science/article/pii/S0920379615302337.
3. R. Prater, C. P. Moeller, R. I. Pinsker, M. Porkolab, O. Meneghini, and V. L. Vdovin, "Application of very high harmonic fast waves for off-axis current drive in the DIII-D and FNSF-AT tokamaks," Nucl. Fusion **54**, 083024 (2014), https://doi.org/10.1088/0029-5515/54/8/083024.
4. C. Lau, E. F. Jaeger, N. Bertelli, L. A. Berry, D. L. Green, M. Murakami, J. M. Park, R. I. Pinsker, and R. Prater, "AORSA full wave calculations of helicon waves in DIII-D and ITER," Nucl. Fusion **58**, 066004 (2018), https://doi.org/10.1088/1741-4326/aab96d.
5. B. V. Compernolle, M. W. Brookman, C. P. Moeller, R. I. Pinsker, A. M. Garofalo, R. O'Neill, D. Geng, A. Nagy, J. P. Squire, K. Schultz, C. Pawley, D. Ponce, A. C. Torrezan, J. Lohr, B. Coriton, E. Hinson, R. Kalling, A. Marinoni, E. H. Martin, R. Nguyen, C. C. Petty, M. Porkolab, T. Raines, J. Ren, C. Rost, O. Schmitz, H. Torreblanca, H. Q. Wang, J. Watkins, and K. Zeller, "The high-power helicon program at DIII-D: gearing up for first experiments," Nucl. Fusion **61**, 116034 (2021), https://doi.org/10.1088/1741-4326/ac25c04.
6. C. T. Holcomb, M. A. Makowski, R. J. Jayakumar, S. A. Allen, R. M. Ellis, R. Geer, D. Behne, K. L. Morris, L. G. Seppala, and J. M. Moller, "Motional stark effect diagnostic expansion on diii-d for enhanced current and e r profile measurements," Rev. Sci. Instrum. **77**, 10E506 (2006), https://doi.org/10.1063/1.2235812.
7. B. Van Compernolle, M. Brookman, C. Moeller, R. Pinsker, A. Garofalo, R. O'Neill, D. Geng, A. Nagy, J. Squire, K. Schultz, *et al.*, "The high-power helicon program at diii-d: gearing up for first experiments," Nuclear Fusion **61**, 116034 (2021).
8. Y. Lin, S. Wukitch, A. Parisot, J. C. Wright, N. Basse, P. Bonoli, E. Edlund, L. Lin, M. Porkolab, G. Schilling, and P. Phillips, "Observation and modelling of ion cyclotron range of frequencies waves in the mode conversion region of alcator c-mod," Plasma Physics and Controlled Fusion **47**, 1207–1228 (2005).
9. E. Nelson-Melby, M. Porkolab, P. T. Bonoli, Y. Lin, A. Mazurenko, and S. J. Wukitch, "Experimental observations of mode-converted ion cyclotron waves in a tokamak plasma by phase contrast imaging," Phys. Rev. Lett. **90**, 155004 (2003).
10. N. Tsujii, M. Porkolab, P. T. Bonoli, E. M. Edlund, P. C. Ennever, Y. Lin, J. C. Wright, S. J. Wukitch, E. F. Jaeger, D. L. Green, and R. W. Harvey, "Validation of full-wave simulations for mode conversion of waves in the ion cyclotron range of frequencies with phase contrast imaging in alcator c-mod," Physics of Plasmas **22**, 082502 (2015), https://doi.org/10.1063/1.4927912.
11. E. M. Davis, J. C. Rost, M. Porkolab, A. Marinoni, and M. A. Van Zeeland, "A combined phase contrast imaging and heterodyne interferometer system for multiscale fluctuation measurements (invited)," Review of Scientific Instruments **89**, 10B106 (2018), https://doi.org/10.1063/1.5035413.
12. A. Marinoni, C. P. Moeller, J. C. Rost, M. Porkolab, and E. M. Edlund, "A Pockels cell enabled heterodyne phase contrast imaging diagnostic for detection of ion cyclotron emission," Rev. Sci. Instrum. **93**, 083502 (2022), https://doi.org/10.1063/5.0101715.
13. E. F. Jaeger, L. A. Berry, E. D'Azevedo, D. B. Batchelor, M. D. Carter, K. F. White, and H. Weitzner, "Advances in full-wave modeling of radio frequency heated, multidimensional plasmas," Phys. Plasmas **9**, 1873 (2002), https://doi.org/10.1063/1.1455001.
14. C. Lau, L. A. Berry, E. F. Jaeger, and N. Bertelli, "Cold plasma finite element wave model for helicon waves," Plasma Phys. Control. Fusion **61**, 045008 (2019), https://doi.org/10.1088/1361-6587/aafd04.
15. E.-H. Kim, M. Ono, S. Shiraiwa, M. Poulos, B. Van Compernolle, and N. Bertelli, "Full-wave simulations of helicon wave coupling optimization and possible parasitic excitation of slow waves near the edge plasma," Bulletin of the American Physical Society (2022).
16. A. P. Smirnov, R. Harvey, and K. Kupfer, "A general ray tracing code GENRAY," Bull Amer. Phys. Soc **39**, 1626 (1994).
17. C. Lau, M. Brookman, A. Dimits, B. Dudson, E. Martin, R. I. Pinsker, M. Thomas, and B. V. Compernolle, "Helicon full-wave modeling with scrape-off-layer turbulence on the DIII-D tokamak," Nucl. Fusion **61**, 126072 (2021), https://doi.org/10.1088/1741-4326/ac36f3.
18. M. Porkolab, R. Pinsker, G. H. DeGrandchamp, S. Baek, B. van Compernolle, S. S. D. Denk, C. C. Petty, S. Tang, and K. Thome, "Parametric decay instabilities driven by high-power helicon waves in DIII-D," Paper P2.18 presented at this conference and references therein (2022).